ACS APPLIED MATERIALS & INTERFACES

Research Article

www.acsami.org

Hierarchically Structured Microspheres for High-Efficiency Rutile TiO_2-Based Dye-Sensitized Solar Cells

Meidan Ye,[†,‡] Dajiang Zheng,[†,‡] Mengye Wang,[†,‡] Chang Chen,[†] Wenming Liao,[‡,§] Changjian Lin,*[,†] and Zhiqun Lin*[,‡]

[†]State Key Laboratory of Physical Chemistry of Solid Surfaces, and Department of Chemistry, College of Chemistry and Chemical Engineering, Xiamen University, Xiamen 361005, China

[‡]School of Materials Science and Engineering, Georgia Institute of Technology, Atlanta, Georgia 30332, United States

[§]School of Chemical Engineering and Technology, Tianjin University, Tianjin, China 30072

Supporting Information

ABSTRACT: Peachlike rutile TiO_2 microsphere films were successfully produced on transparent conducting fluorine-doped tin oxide substrate via a facile, one-pot chemical bath route at low temperature (T = 80−85 °C) by introducing polyethylene glycol (PEG) as steric dispersant. The formation of TiO_2 microspheres composed of nanoneedles was attributed to the acidic medium for the growth of 1D needle-shaped building blocks where the steric interaction of PEG reduced the aggregation of TiO_2 nanoneedles and the Ostwald ripening process. Dye-sensitized solar cells (DSSCs) assembled by employing these complex rutile TiO_2 microspheres as photoanodes exhibited a light-to-electricity conversion efficiency of 2.55%. It was further improved to a considerably high efficiency of 5.25% upon a series of post-treatments (i.e., calcination, $TiCl_4$ treatment, and O_2 plasma exposure) as a direct consequence of the well-crystallized TiO_2 for fast electron transport, the enhanced capacity of dye loading, the effective light scattering, and trapping from microstructures.

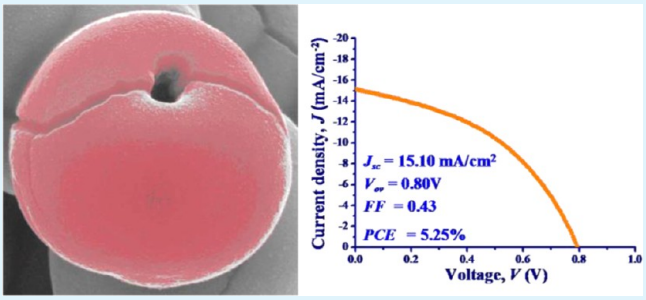

KEYWORDS: *rutile TiO_2 microspheres, low-temperature synthesis, chemical bath method, dye-sensitized solar cells, post-treatments, light-to-electricity conversion efficiency*

INTRODUCTION

Because of its outstanding chemical and physical properties, including chemical stability, photostability and appropriate electronic band structure, TiO_2 has received extensive attention as a promising candidate for use in water splitting, photocatalysis, sensors, and dye-sensitized solar cells (DSSCs) over the past decades.[1−7] The ability to tune nanostructured TiO_2 to different morphologies and polymorphs is the key to effectively realize aforementioned applications, as its optical and electrical properties depend critically on the shape, size, and phase of TiO_2.[8−12] TiO_2 exists mainly in four crystal structures: anatase, rutile, brookite, and TiO_2 (B). Different phases possess different physicochemical properties offering different functionalities. Among these four phases, rutile and anatase are the most practically important crystal structures. In the photocatalytic applications, anatase usually exhibits higher activity than rutile because of the lower electron mobility and the greater electron−hole recombination in rutile.[13,14] However, rutile (3.02 eV) has a smaller band gap than anatase (3.20 eV), leading partially to a photoresponse extending slightly into the visible light region. Moreover, rutile is the most thermodynamically stable and has high refractive index and good light-reflecting properties.[11,14,15] Strikingly, when mixing them together, the synergistic effect between anatase and rutile phases induces the spatial charge separation and reduces the electron−hole recombination, leading to enhanced photocatalytic efficiency.[12,16] Notably, the most commercially active photocatalyst Degussa P25 is a mixture of anatase and rutile phases.[5,13,17]

In addition, TiO_2 nanocrystals with various morphologies, such as nanorods, nanotubes, nanowires, nanosheets, nanospheres, etc., have been obtained by many synthetic approaches, including sol-gel synthesis, chemical bath method, hydrothermal process, chemical/physical vapor deposition, electrochemical anodization.[18−26] Among these techniques, low temperature and atmospheric pressure synthetic strategies are highly desirable primarily due to the use of relatively simple reaction equipment, safe operation, and low fabrication cost.[16,27] Accordingly, much work has centered on the preparation of crystalline TiO_2 nanostructures in moderate conditions.[8,9,16,28] For example, rod-shaped rutile nanocrystals were prepared by thermohydrolysis of titanium(IV) chloride in

Received: November 28, 2013
Accepted: January 27, 2014
Published: January 27, 2014

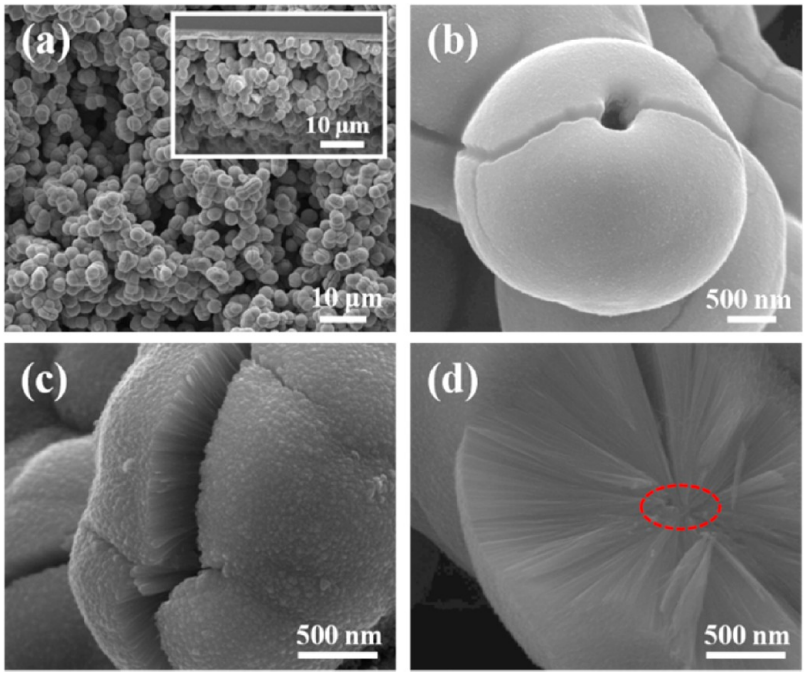

Figure 1. SEM images of the TiO_2 microsphere film on the FTO glass substrate prepared by a chemical bath process for 12 h: (a) microspheres over a large area (inset: the cross-sectional view); (b) a full-grown microsphere; (c) surface of the microsphere; and (d) inside of the microsphere (red dashed line marked the solid core of microspheres).

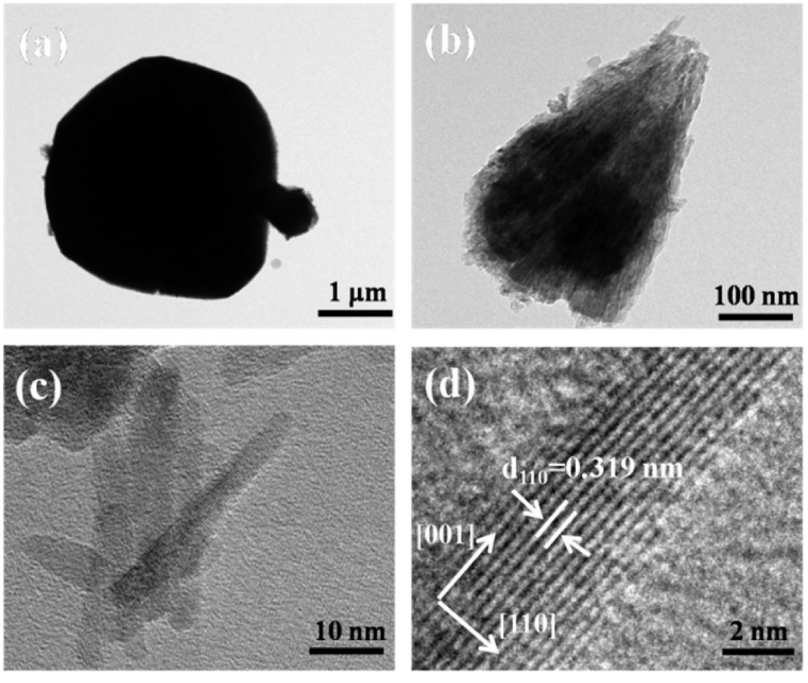

Figure 2. TEM images of TiO_2 microsphere prepared by a chemical bath process for 12 h: (a) a fully grown microsphere; (b) a small portion taken from the microsphere; (c) nanoneedle building blocks within microsphere; (d) HRTEM image of a TiO_2 nanoneedle.

hydrochloric acid/alcohol aqueous solution at 40−90 °C.[8] The anatase TiO_2 nanocrystals with various shapes obtained from controlled aqueous sol−gel reaction at room temperature showed superior photocatalytic activities.[27]

To date, zero-dimensional (0D), one-dimensional (1D) and two-dimensional (2D) TiO_2 nanostructures are routinely synthesized in a large scale by various physical and chemical routes.[29−31] Notably, 3D TiO_2 architectures assembled with enormous 0D, 1D, or 2D morphologies have attracted intensive interest as they combine the feature of nanoscopic building blocks (i.e., unique physicochemical properties and large areas) and the benefit of microscopic structures (i.e., advantageous scattering effect for light harvesting and easy handling), and thus have potential applications in photocatalysts and DSSCs.[9,32−34] Recently, 3D TiO_2 architectures composed of nanoparticles, nanorods, nanowires, nanosheets and nanotubes have been reported.[10,32,33,35−37] For instance, F-containing anatase TiO_2 hollow microspheres shaped by aggregating

several nanoflakes were obtained by hydrothermal treatment of TiF_4 in H_2SO_4 aqueous solution at 160 °C and exhibited excellent performance in photocatalysis of methyl blue (MB).[36] Furthermore, DSSCs based on the TiO_2 nanobranched arrays prepared via a two-step synthesis showed a power conversion efficiency of 3.75%, because of the increase in dye adsorption and light harvesting efficiency.[38] However, it is noteworthy that the fabrication of these complex superstructures often requires stringent conditions, especially high temperature and high pressure.[32,33,36,38,39]

Herein, we report the direct formation of well-defined peach-like rutile TiO_2 microspheres on fluorine-doped tin oxide (FTO) substrate via a simple, one-step low-temperature chemical bath route under atmospheric pressure. The well-defined microspheres comprising of massive nanoneedles (i.e., hierarchically structured TiO_2 microspheres) provided high surface area for dye adsorption and effective light scattering, yielding DSSCs with a power conversion efficiency (PCE) of 2.55%. Remarkably, subsequent calcination, $TiCl_4$ treatment and O_2 plasma exposure rendered a markedly improved PCE of 5.25% as a direct consequence of well-crystallized TiO_2 for fast electron transport, the improved dye loading, the effective light scattering and trapping from microspheres.

Figure 1a displays a representative field emission scanning electron microscopy (FESEM) image of TiO_2 microsphere film prepared in a chemical bath reaction containing a mixture of 15 mL of H_2O, 5 mL of ethanol, 5 mL of concentrated hydrochloric acid, 0.50 mL of TTIP, and 0.50 g of PEG14000 at 80−85 °C for 12 h. Such film densely distributed over the entire surface of the FTO substrate. It consisted of large quantities of microspheres (Figure 1a) with a thickness of approximately 30 μm (inset in Figure 1a). A close-up of a fully grown microsphere revealed the microsphere had a round peachlike feature with a cavity on the top of the surface. Some cracks on the surface were also clearly evident (Figure 1b). Close examination showed that the microspheres possessed rough surface (Figure 1c) and was made of numerous slender subunits (i.e., needle-shaped building blocks) with an approximately 1.5 μm long and radially oriented with their growth axes spreading from a solid core (red circle in Figure 1d, i.e., possessing hierarchical architectures).

To examine the detailed structure of an individual microsphere, we performed transmission electron microscopy (TEM). The sample was subjected to mild ultrasonication in ethanol solution to yield an individual microsphere. Interestingly, Figure 2a shows a single microsphere with a diameter of 2−3 μm (Figure 2a), which accidentally happened to be decorated with a short rod on its top when prepared via the ultrasonication. Each microsphere was composed of numerous parallel nanoneedles with diameters in a range of 5−10 nm (Figures 2b and 2c). More importantly, these nanoneedles were completely crystalline as confirmed by high-resolution TEM (HRTEM). The lattice fringe with interplanar spacing of d_{110} = 3.19 Å can be indexed to tetragonal rutile phase (Figure 2d). In general, the (110) crystal plane is perpendicular to the (001) crystal plane, and thus the nanoneedles grew along the (110) crystal plane with a preferred [001] orientation.[40]

Moreover, Figure 3 shows the Raman spectrum of TiO_2 microspheres prepared by chemical bath process for 12 h, indicating that the as-prepared sample possesses rutile phase according to the characteristic Raman modes at 132 cm^{-1} (B_{1g}), 440 cm^{-1} (E_g), and 608 cm^{-1} (A_{1g}) with a broad band near 240 cm^{-1} assigned to a second-order phonon.[41,42]

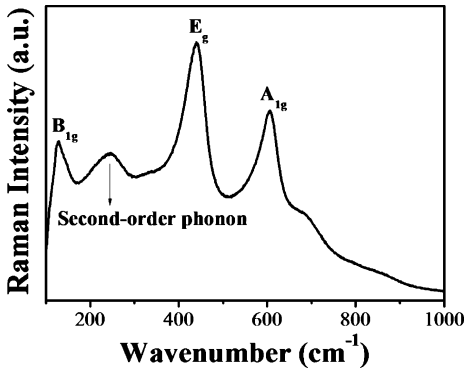

Figure 3. Raman spectrum of TiO_2 microsphere film prepared by chemical bath process for 12 h.

The X-ray diffraction (XRD) analysis also showed that the microsphere films were pure rutile TiO_2. As shown in Figure 4,

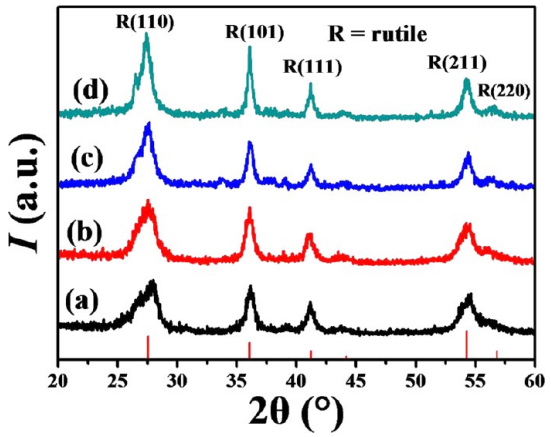

Figure 4. XRD patterns of TiO_2 microsphere films prepared via the chemical bath process for different times: (a) 3, (b) 6, (c) 9, and (d) 12 h. Red vertical lines in the figure represent the standard XRD pattern of rutile (JCPDS No.01-1292).

microsphere films prepared under typical reaction conditions for different times possessed the same diffraction peaks regardless of the difference in intensity, and can be assigned to tetragonal rutile phase with the diffraction peaks at 2θ = 27.4, 36.1, 41.2, 54.3, and 56.6°, corresponding to the (110), (101), (111), (211), and (220) crystal faces of rutile TiO_2 (space group, $P4_2/mnm$; JCPDS No. 01-1292, $a = b$ = 0.459 nm and c = 0.295 nm), in accordance with the HRTEM measurement (Figure 2d) and the Raman result (Figure 3). In the work that follows, the growth parameters were scrutinized in order to reveal the prominent factors that governed the formation of hierarchical architectures.

As displayed in Figure S1 (see the Supporting Information), in the absence of both PEG14000 and ethanol, the formed film consisted of large agglomerates fused together (Figure S1a). The agglomeration was also observed when only 5 mL ethanol was added (see Figure S1b and Figure S4a in the Supporting Information). In contrast, well-defined microspheres clearly appeared over a large scale when produced in the presence of 0.50 g of PEG14000 only (see Figure S1c in the Supporting Information), implying that the addition of PEG14000 favorably assisted the formation of discrete microspheres. Furthermore, the addition of both PEG14000 and ethanol promoted the production of much more elaborate micro-

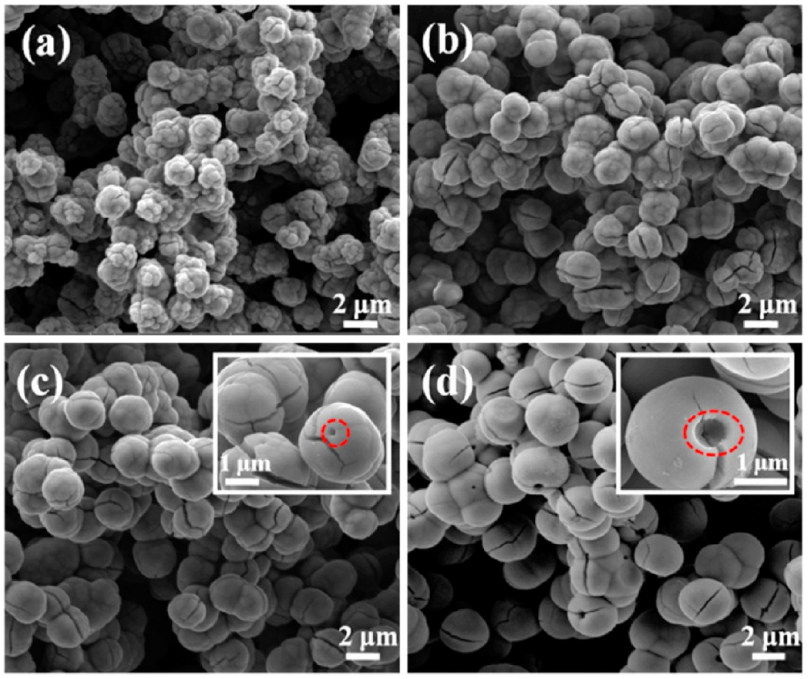

Figure 5. SEM images of TiO_2 microspheres prepared by a chemical bath process for different times: (a) 3, (b) 6, and (c) 9 h (inset: the microsphere with a cavity); and (d) 12 h (inset: the microsphere with a cavity).

spheres (Figure 5d). However, some microspheres still unavoidably connected together during the growth (Figure 5d). In other control experiments, on the one hand, reducing the amount of PEG14000 to 0.25 g resulted in larger microspheres (see Figure S2a in the Supporting Information), whereas increasing its amount to 1.00 g introduced broken microspheres composed of several smaller spheres (see Figure S2b in the Supporting Information). Obviously, the presence of PEG14000 significantly disrupted the agglomerated TiO_2 nanocrystals and markedly imparted the formation of versatile hierarchical architectures as a function of the concentration of PEG14000. On the other hand, the growth temperature also critically influenced the microsphere organization. Inevitably, decreasing the growth temperature down to 70 °C yielded the aggregated microspheres (see Figure S2c in the Supporting Information). Additionally, lower concentration of TTIP precursors gave rise to small particulate microspheres (see Figure S2d in the Supporting Information), whereas higher precursor concentration induced larger microspheres (see Figure S2e in the Supporting Information). This is not surprising as the precursor concentration affected the hydrolysis rate of Ti^{4+}, which in turn greatly impacted the nucleation density, leading to the largely different hierarchically structured TiO_2 microspheres. Similarly, reducing the volume of HCl down to 1 mL promoted the quick hydrolysis of precursors, leaving almost nothing on the FTO substrate; however, increasing the acid volume to 10 mL yielded flower-like morphology comprising several short nanorods (see Figure S2f in the Supporting Information) because of the vigorous suppression of Ti^{4+} hydrolysis under high acidity condition.

In our time-dependent study, it showed that the Ostwald ripening occurred during the chemical bath process. Specifically, the nanocrystals were emerged readily after 1.5 h (see Figure S3a in the Supporting Information). The microspheres spread completely over the FTO substrate after 3 h (Figure 5a). The diameter of formed microspheres was then gradually increased from roughly 1 to 3 μm; and concurrently, the microspheres evolved into clear peachlike features as the time progressed from 6 h to 12 h (Figure 5). In comparison to that obtained at 12 h (Figure 5d), the prolonged growth to 15 h yielded an almost similar microsphere feature and film thickness (see Figure S3b and Table S1 in the Supporting Information), suggesting that the TTIP precursor was almost completely consumed and the size of microspheres was nearly stable after 12 h. Moreover, the peak intensities in XRD patterns were progressively increased (Figure 4), which was associated with the increase in the film thickness and the degree of crystallization. The film thickness was increased from 10 to 30 μm, whereas the crystal size coarsened from 10 to 15 nm (calculated according to the Scherrer equation), as the reaction proceeded from 3 to 15 h (see Table S1 and Figure S4b in the Supporting Information). In the Ostwald ripening process, the smaller and less crystalline or less dense structure would be dissolved gradually, while the larger and better crystallized or denser structure would grow.[43,44] Thus, within the microspheres, prolonged growth time yielded better crystallized TiO_2 nanocrystals that grew larger at the expense of smaller and less crystalline TiO_2 nanocrystals. Consequently, the crystallinity and the diameter of microspheres along with their film thickness were all increased during the course of crystal growth, dissolution and redeposition. Interestingly, a circular cavity with a diameter of 200 nm on the top of microsphere was apparently emerged after 9 h (marked in red cycle in the inset of Figure 5c), which increased to 700 nm after 12 h (red cycle in the inset of Figure 5d). The formation of these cavities could be ascribed to the crystal dissolution in the Ostwald ripening process, namely, some less-crystalline sites with more defects on the microsphere surface were preferentially dissolved.[45,46] We note that the appearance of surface cracks (Figure 1c) is expected to reduce the surface tension of microsphere and retain its lowest energy as the minimization in surface energy is

dx.doi.org/10.1021/am405442n | ACS Appl. Mater. Interfaces 2014, 6, 2893−2901

the dominant driving force for the crystal growth and structure evolution.[47]

In the present study, FTO glasses were used as substrates to support TiO_2 films as they possess a tetragonal rutile structure and the small lattice mismatch (only 2%) between the tetragonal FTO ($a = b = 0.4687$ nm) and rutile TiO_2 ($a = b = 0.4594$ nm).[40] Such small lattice mismatch promoted the epitaxial nucleation and growth of rutile TiO_2 film compactly on the FTO substrate with a close interaction, which is highly desirable to effectively transfer the excited electrons from TiO_2 to the FTO substrate for high-performance DSSCs. In addition, because of the presence of HCl in the precursor, the formation of 1D TiO_2 nanostructures (e.g., rods or needles) instead of 3D nanoparticles was favored as the (110) plane of rutile has a positive polar-face and Cl^- can be preferentially adsorbed on its surface to restrain the contact of the TiO_2 grains with the (110) surface, and thus the crystal growth along the [110] direction was greatly retarded, while accelerated in the [001] direction, thereby forming nanoneedle-like building blocks.[40,48] These nanoneedles, however, can aggregate together to reduce the overall surface energy and reach a stable state by forming an agglomerated shape. To this end, PEG14000 was employed to interrupt the agglomeration. It is well known that that PEG is an inexpensive, nontoxic, nonvolatile and nonionic surfactant with excellent water-solubility, lubricating property and high stability at room temperature.[49] Moreover, PEG is available in a wide molecular weight distribution (in the range of 200−20 000) and different chain length with diverse frameworks, which ultimately provide different assembling effects on the final products. More importantly, PEG contains hydrophilic groups (i.e., −OH end group and −O− along the chain), which can effectively act as a donor to metal ions to form metal complexes with diverse conformations, and precisely control the morphology of the resulting materials.[44,50−53] Therefore, PEG has been widely utilized in the synthesis of a number of materials, including TiO_2, ZnO, and $CaCO_3$.[28,51−54] In this work, PEG14000 is considered as a steric dispersant that prevent the agglomeration of TiO_2 microspheres, while ethanol acts to facilitate the dissolution of PEG14000. It is worth noting that the O atom in PEG has loose coordination ability with metal ions, which renders PEG to adsorb onto the surface of primary TiO_2 nanocrystals to reduce the surface tension, and at the same time the adsorbed PEG with long organic chains on the TiO_2 surface impose a steric interaction to slow down the precursor hydrolysis rate and alleviate the agglomeration during the crystal growth.[44,53] As a result, the reduced agglomeration favored the formation of well-defined microsphere architecture. Notably, secondary nucleation can occur preferentially on the active sites with more defects of the as-grown microspheres.[48,55] Thus, it is not surprising that several individual microspheres grew up conjointly, and ultimately connected one another in the form of microsphere clusters.

All TiO_2 microsphere films noted above were then utilized as photoanodes to produce DSSCs, and their performance was measured (see Experimental Section). Table 1 and Table S2 in the Supporting Information summarize the device performance of the resulting N719 dye-sensitized rutile TiO_2-based solar cells, where the representative current−voltage (J−V) characteristics are shown in Figure 6. In DSSCs, the amount of dye loading, the light harvesting and the efficient charge separation and transport have crucial influences on the light-to-electricity conversion efficiency of DSSCs. In this context, first, we surveyed the devices produced using rutile TiO_2 that were prepared under different experimental conditions but without any post-treatments (Table 1 and Table S2 in the Supporting Information); the optimal microsphere film yielded with the assistance of PEG14000 in TiO_2 precursor was found to show

Table 1. Summary of Device Performance of Dye-Sensitized Solar Cells Based on Rutile TiO_2 Microsphere Films Prepared under Different Conditions

sample	J_{sc} (mA/cm^2)	V_{oc} (V)	FF	PCE (%)
3 h	3.91	0.68	0.53	1.41
6 h	4.86	0.71	0.56	1.92
9 h	5.70	0.76	0.49	2.13
12 h	6.58	0.80	0.48	2.55
15 h	6.40	0.75	0.53	2.52
12 h/450 °C	8.71	0.82	0.42	3.02
12 h/600 °C	10.55	0.85	0.43	3.89
12 h/600 °C/$TiCl_4$	13.97	0.83	0.41	4.77
12 h/600 °C/$TiCl_4$/O_2	15.10	0.80	0.43	5.25

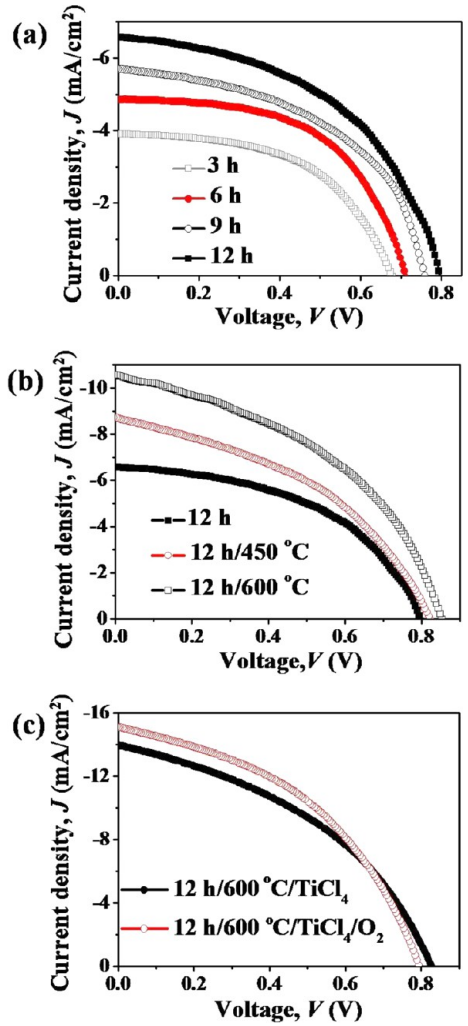

Figure 6. J−V characteristics of DSSCs capitalizing on TiO_2 microsphere films as photoanodes. (a) The TiO_2 microsphere films prepared by a chemical bath process for different times: 3, 6, 9, and 12 h. (b) The TiO_2 microsphere films grown for 12 h without annealing, with annealing at 450 °C, and with annealing at 600 °C. (c) The TiO_2 microsphere films grown for 12 h and then annealed at 600 °C, followed by $TiCl_4$ treatment, and under the same treatment as previous, followed by the last step of O_2 plasma exposure.

dx.doi.org/10.1021/am405442n | ACS Appl. Mater. Interfaces 2014, 6, 2893−2901

the highest device performance, exhibiting an open circuit voltage V_{oc} of 0.80 V, a short circuit current J_{sc} of 6.58 mA/cm^2, a fill factor FF of 0.48, and a power conversion efficiency PCE of 2.55% (Table 1 and Figure 6a), and representing a 46% increase in PCE as compared to the samples prepared in absence of PEG14000 (PCE = 1.75%, J_{sc} = 5.99 mA/cm^2, V_{oc} = 0.74 V, FF = 0.39, Table S2 in the Supporting Information). Such a performance enhancement (i.e., PCE = 2.55%) can be attributed to the larger surface area for more dye uptake (see Table S1 in the Supporting Information), in combination with the increased crystallization (Figure S4a) and improved light harvesting because of the hierarchical structures (Figure 7a). We note that as the growth time progressed, the thickness (see Table S1 in the Supporting Information) and crystallization (Figure 4) of TiO_2 films were increased simultaneously, which contributed higher dye adsorption (i.e. the amount of dye loading increased from 1.38×10^{-8} mol/cm^2 to 2.71×10^{-8} mol/cm^2 when the growth time increased from 3 h to 12 h, Table S1 in the Supporting Information) and fast electron transport, and thus higher performance of the corresponding DSSCs (i.e., PCE improved from 1.41% for the 3 h TiO_2 microsphere film to 2.55% for the 12 h TiO_2 microsphere film, Table 1 and Figure 6a). As noted above, when the growth was up to 12 h, the films tended to be stable due to the equilibrium between the crystal growth and the dissolution process (see Tables S1 and S2 in the Supporting Information). Therefore, the microsphere films prepared from the 12 h chemical bath reaction was chosen to conduct the further studies as discussed below.

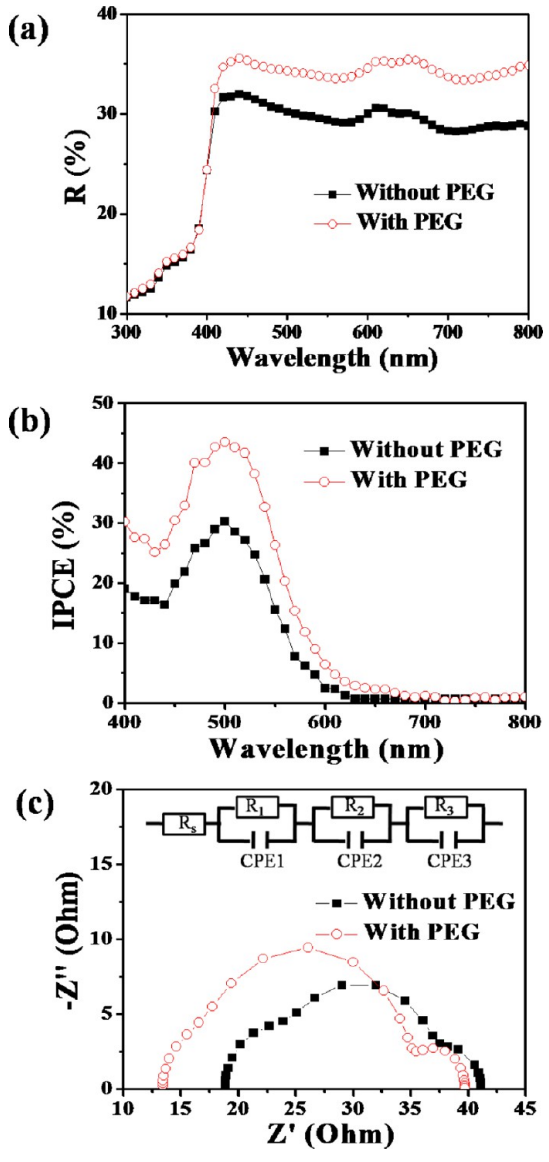

Figure 7. (a) UV−vis diffuse reflectance spectra, (b) IPCE spectra, and (c) Nyquist plots (fitted based on the equivalent circuit shown as the inset) of rutile TiO_2 microsphere film prepared by a chemical bath process for 12 h without and with the presence of 0.50 g of PEG14000, respectively.

Second, in order to increase the crystallinity of TiO_2 nanocrystals for fast electron transport in DSSCs, the above optimal microsphere films (i.e., with PCE = 2.55%) were then calcined. As clearly evident in Figure S4c, the crystallization of rutile phase was improved after calcined at either 450 °C or 600 °C. Accordingly, this thermal modification greatly raised the PCE from 2.55% to 3.02% (J_{sc} = 8.71 mA/cm^2, V_{oc} = 0.82 V, FF = 0.42) for calcination at 450 °C, and to 3.89% (J_{sc} = 10.55 mA/cm^2, V_{oc} = 0.85 V, FF = 0.43) for calcination at 600 °C (Table 1 and Figure 6b), respectively. However, the calcination also led to the formation of bigger crystals with a slightly lower surface area (see Table S1 in the Supporting Information), as reported in literature.[8,14] It is well-documented that when amorphous TiO_2 is thermally annealed below 500 °C, the anatase phase will be formed.[56] This is also confirmed in this work when the samples were treated with $TiCl_4$ solution to decorate amorphous TiO_2 nanoparticles on the microsphere film surface that had been calcined at 600 °C, followed by the calcination again at 450 °C (Figure S4d), the anatase phase was emerged as evidenced in the XRD measurement (Figure S4d). However, when calcined the as-prepared TiO_2 microspheres without $TiCl_4$ treatment at 450 °C, no anatase phase appeared (see Figure S4c in the Supporting Information). This result implies that the microsphere film even without any calcination was already in its complete crystallization state of rutile phase, but with many defects in the film prepared at low temperature; thus, the calcination process was performed to increase their crystallinity.

Third, as noted above, $TiCl_4$ treatment followed by a 450 °C calcination additionally deposit many anatase nanoparticles on the microsphere surface (see Figure S3c in the Supporting Information). Clearly, this decoration certainly increased the amount of dye uptake from 2.59 × 10^{-8} mol/cm^2 to 2.88 × 10^{-8} mol/cm^2 for the corresponding samples (see Table S1 in the Supporting Information), suggesting an 11% increase in the dye capacity. Thus, the $TiCl_4$-treated DSSC showed an enhanced PCE of 4.77% (J_{sc} = 13.97 mA/cm^2, V_{oc} = 0.83 V, *FF* = 0.41, Table 1 and Figure 6c), representing a 23% increase in PCE (as compared to PCE = 3.89% for non-$TiCl_4$ treated device).

Finally, to further improve the device efficiency of DSSCs, we exposed microsphere films to O_2 plasma prior to the immersion of the films into the N719 dye solution. We have previously reported that upon the exposure to O_2 plasma, the density of hydroxyl groups on the TiO_2 surface increased and eventually saturated; this increased the amount of dye loading due to the coupling reaction between terminal carboxylic acid groups on N719 and complementary hydroxyl groups on the TiO_2 surface, thus significantly regulating the charge transfer from the N719 dye to TiO_2.[24] In the present study, a 10 min O_2 plasma exposure was applied according to our previous work.[24]

As a result, the amount of dye adsorption was increased from 2.88×10^{-8} mol/cm^2 to 3.06×10^{-8} mol/cm^2, reflecting an improvement in PCE of the resulting DSSCs from 4.77% without the O_2 plasma treatment to 5.25% after the O_2 plasma exposure (J_{sc} = 15.10 mA/cm^2, V_{oc} = 0.80 V, FF = 0.43, Table 1 and Figure 6c).

As described above, the addition of PEG rendered the formation of well-defined TiO_2 microspheres. Moreover, the device efficiency of DSSCs based on the PEG-facilitated TiO_2 microsphere films (denoted as Cell I; PCE = 2.55%, Table 1) was higher than that (PCE = 1.75%, see Table S2 in the Supporting Information) using the TiO_2 microsphere film prepared in the absence of PEG (denoted as Cell II). In order to understand the different photovoltaic performance of these two DSSCs, in addition to the dye loading measurement (see Table S1 in the Supporting Information) and the UV−vis diffuse reflectance spectra (Figure 7a), the incident-photon-to-current efficiency (IPCE) studies were also performed (Figure 7b). The IPCE at 510 nm for Cell I (red hollow cycle, 43%) was higher than that of Cell II (black solid tetragonal, 30%). Moreover, the IPCE over the entire wavelength region for Cell I was also higher than that of Cell II, suggesting the increased light harvesting for the well-defined hierarchically structured TiO_2 microspheres (i.e., the PEG-facilitated TiO_2 microsphere films).

Electrochemical impedance spectroscopy (EIS) measurements were conducted in order to further elucidate the electrochemical characteristics of the two aforementioned DSSCs. The Nyquist plots for these two DSSCs are shown in Figure 7c. The fitted results are summarized in Table S3 in the Supporting Information. The EIS spectra exhibited three semicircles with a contact series resistance (R_s) on the FTO substrate. The first semicircle in the high frequency range is related to the resistance at the counter electrode (R_1) for the reduction reaction of I_3^- in the electrolyte using Pt as the counter electrode. The second semicircle in the intermediate frequency range represents the charge recombination resistance (R_2) at interfaces among the electrolyte, dye, and TiO_2. The third semicircle in the low frequency range offers the information regarding the resistance of finite diffusion of the electrolyte (R_3).[3]The close R_1 of 3.89 Ω and 3.73 Ω for the Cell I and Cell II, respectively were obtained as the counter electrodes (i.e., Pt) were prepared in the nearly same manner. Intriguingly, the smaller R_s of 13.43 Ω and larger R_2 of 17.96 Ω for Cell I than the corresponding resistances for Cell II (i.e., R_s = 18.86 Ω and R_2 = 12.80 Ω) signified a better contact of TiO_2 microspheres with the FTO substrate and lower recombination rate for faster charge transport, respectively for Cell I. Finally, a smaller R_3 of 4.61 Ω for Cell I than that of 5.58 Ω for Cell II was found, implying a superior mass diffusion channel for the hierarchical structure in Cell I (Figure 1a), as compared to the agglomerated structure in Cell II (see Figure S1b in the Supporting Information).

In summary, intriguing hierarchically structured rutile TiO_2 microspheres composed of nanoneedles were crafted via a simple, one-step and low temperature chemical bath route. Such hierarchical architecture carried advantageous features, including large surface area and effective light scattering and trapping due to the well-defined hierarchical structures. When they were exploited as the photoanodes in DSSCs, the resulting devices exhibited a PCE of 2.55% despite the rutile nature of TiO_2 microspheres, which was further increased to 5.25% upon sequential modifications of TiO_2 (i.e., calcination, $TiCl_4$ treatment, and O_2 plasma exposure). The PCE can be further improved by tuning the reaction condition in chemical bath process or employing other post-treatments (e.g., etching treatment) to produce TiO_2 microspheres with higher surface area. Importantly, the viable chemical bath process enables the creation of crystallized hierarchical rutile TiO_2 structures directly on large transparent conducting substrates at low temperature, which are highly desirable for practical applications in photocatalysis and solar cells, among other areas.

EXPERIMENTAL SECTION

Formation of Hierarchically Structured TiO_2 Materials. Peachlike rutile TiO_2 microsphere films on transparent conducting FTO substrate were prepared via a chemical bath route. In a typical synthesis, 0.50 g polyethylene glycol (PEG, M_w = 14,000, denoted PEG14000, PDI = 1.1) was dissolved in a mixture of 5 mL ethanol and 15 mL deionized water, which was further added with 5 mL concentrated hydrochloric acid (HCl; mass fraction =36-38%). The mixture was stirred under ambient condition for 5 min before adding 0.50 mL titanium isopropoxide (TTIP-TiO_2 precursor; Sigma-Aldrich Co.). After stirring for an additional 5 min, the transparent solution was transferred into a glass bottle with a lid but without being sealed. Subsequently, an FTO substrate (F:SnO_2, 2 cm × 2 cm, 14 Ω/square; Pilkington Glass, USA) ultrasonically cleaned for 30 min in a mixed solution of acetone and ethanol with a 1:1 volume ratio, followed by deionized water rinsing for 15 min, was placed in the transparent solution with the conducting side of FTO facing up. The reaction was allowed to proceed at 80−85 °C for 12 h in an oven. The bottle was then cooled to room temperature in air. Subsequently, the FTO substrate was taken out, rinsed extensively with deionized water, and dried in air. The effects of growth parameters, including the growth time (from 1.5 to 15 h), the initial concentrations of precursor and PEG14000, the alcohol types, the growth temperature (from 70 to 85 °C), and the acidity of reaction solution on the resulting hierarchical structures were systematically investigated. TiO_2 films were also fabricated under the same condition without the addition of PEG14000 as controls to assess the influence of the presence of PEG14000 on the formation of hierarchical architectures.

TiO_2 Solar Cell Fabrication. Dye-sensitized solar cells (DSSCs) were assembled using hierarchically structured TiO_2 films grown on the FTO glass as photoanodes. To improve their crystallinity, the TiO_2 films were annealed at 450 or 600 °C for 2 h inside a furnace. Prior to dye adsorption, the photoanodes were placed in 100 mL of 0.2 M $TiCl_4$ solution at 70 °C for 1 h. After being rinsed with deionized water, the $TiCl_4$-treated sample was annealed at 450 °C for 30 min, followed by a 10 min O_2 plasma exposure. The sample was then soaked in anhydrous ethanol containing 0.2 mM commercially available N719 dye (cis-bis(isothiocyanato)-bis(2,2′-bipyridyl-4,4′-dicarboxylato)ruthenium(II) bis(tetrabutylammonium); Solaronix Co.), and kept for 24 h at room temperature. Platinum (Pt)-coated counter electrode was prepared by dropping 0.5 mM H_2PtCl_6 isopropanol solution on another piece of FTO glass, followed by heating at 400 °C for 20 min. The dye-sensitized TiO_2 film with an active area of approximately 0.12 cm^2 was assembled together with the Pt-coated FTO glass by applying a 25 μm thick hot-melt sealed film as the spacer (SX1170-25; Solaronix). The redox electrolyte used in the study was an ionic liquid containing 0.60 M 1-butyl-3-methylimidazolium iodide (BMIM-I), 0.03 M I_2, 0.50 M 4-tert-butylpyridine (TBP), and 0.10 M guandinethiocyanate (GTC) in a mixture of acetonitrile and valeronitrile (v/v = 85/15) (No. ES-0004, purchased from io.li.tec, Germany). The electrolyte was injected between two electrodes and driven by capillary force through the hole on the hot-melt sealed film.[24]

Characterization. The morphology and lattice structure of TiO_2 films were examined by field emission scanning electron microscopy (FESEM; FEI Quanta250, operated at 10 kV in high vacuum) and transmission electron microscopy (TEM; JEOL 2100, operated at 200 kV). Raman spectrum was recorded on a Renishaw Raman

microspectrometer system 2000 equipped with a He−Ne laser (632.8 nm).Phase identification of TiO_2 was conducted by X-ray diffraction (XRD; SCINTAG XDS-2000, Cu Kα radiation). The light absorption of TiO_2 films and the dye desorption were measured by UV-visible spectroscopy (Varian; UV-Visible spectrophotometer, Cary 5000). The current−voltage (J−V) characteristics were measured using a Keithley Model 2400 multisource meter. A solar simulator (SoLux Solar Simulator) was used to simulate sunlight for an illumination intensity of 100 mW/cm^2 calibrated with a Daystar Meter.The incident-photon-to-current efficiency (IPCE) spectra were measured as a function of wavelength (from 400−800 nm) on the basis of a monochromator (Oriel, model 74125). Impedance tests were performed in dark under open circuit voltage over the frequency range between 1×10^5 and 1×10^{-2} Hz, with an AC voltage magnitude of 10 mV. The impedance data were analyzed by Autolab electrochemical EIS fitting software.

■ ASSOCIATED CONTENT

Supporting Information

FESEM images of TiO_2 films prepared from other control experiments, tables of dye adsorption, device performance of DSSCs, and EIS parameters obtained by fitting the experiment data, and XRD patterns of TiO_2 microsphere films prepared under different experimental conditions. This material is available free of charge via the Internet at http://pubs.acs.org.

■ AUTHOR INFORMATION

Corresponding Authors

*E-mail: cjlin@xmu.edu.cn.

*E-mail: zhiqun.lin@mse.gatech.edu.

Notes

The authors declare no competing financial interest.

■ ACKNOWLEDGMENTS

M.Y., D.Z., and M.W. gratefully acknowledge the financial support from the Chinese Scholarship Council. This work is supported by the National Natural Science Foundation of China (51072170, 21021002) and the National Basic Research Program of China (2012CB932900) (C.L.), and Minjiang Scholar Program and Georgia Institute of Technology (Z.L.).

■ REFERENCES

(1) Ye, M. D.; Gong, J. J.; Lai, Y. K.; Lin, C. J.; Lin, Z. Q. High-Efficiency Photoelectrocatalytic Hydrogen Generation Enabled by Palladium Quantum Dots-Sensitized TiO_2 Nanotube Arrays. *J. Am. Chem. Soc.* **2012**, *134*, 15720−15723.

(2) Wang, M.; Sun, L.; Lin, Z.; Cai, J.; Xie, K.; Lin, C. p−n Heterojunction photoelectrodes composed of Cu_2O-loaded TiO_2 nanotube arrays with enhanced photoelectrochemical and photoelectrocatalytic activities. *Energy Environ. Sci.* **2013**, *6*, 1211−1220.

(3) Ye, M.; Zheng, D.; Lv, M.; Chen, C.; Lin, C.; Lin, Z. Hierarchically Structured Nanotubes for Highly Efficient Dye-Sensitized Solar Cells. *Adv. Mater.* **2013**, *25*, 3039−3044.

(4) Ye, M. D.; Xin, X. K.; Lin, C. J.; Lin, Z. Q. High Efficiency Dye-Sensitized Solar Cells Based on Hierarchically Structured Nanotubes. *Nano Lett.* **2011**, *11*, 3214−3220.

(5) Jang, Y. H.; Xin, X.; Byun, M.; Jang, Y. J.; Lin, Z.; Kim, D. H. An Unconventional Route to High-Efficiency Dye-Sensitized Solar Cells via Embedding Graphitic Thin Films into TiO_2 Nanoparticle Photoanode. *Nano Lett.* **2011**, *12*, 479−485.

(6) Xin, X.; He, M.; Han, W.; Jung, J.; Lin, Z. Low-Cost Copper Zinc Tin Sulfide Counter Electrodes for High-Efficiency Dye-Sensitized Solar Cells. *Angew. Chem., Int. Ed.* **2011**, *50*, 11739−11742.

(7) O'regan, B.; Grfitzeli, M. A Low-Cost, High-Efficiency Solar Cell Based on Dye-Sensitized. *Nature* **1991**, *353*, 737−740.

(8) Wang, W.; Gu, B. H.; Liang, L. Y.; Hamilton, W. A.; Wesolowski, D. J. Synthesis of Rutile (alpha-TiO_2) Nanocrystals with Controlled Size and Shape by Low-Temperature Hydrolysis: Effects of Solvent Composition. *J. Phys. Chem. B* **2004**, *108*, 14789−14792.

(9) Masuda, Y.; Ohji, T.; Kato, K. Multineedle TiO_2 Nanostructures, Self-Assembled Surface Coatings, and Their Novel Properties. *Cryst. Growth Des.* **2010**, *10*, 913−922.

(10) Wang, C. X.; Yin, L. W.; Zhang, L. Y.; Qi, Y. X.; Lun, N.; Liu, N. N. Large Scale Synthesis and Gas-Sensing Properties of Anatase TiO_2 Three-Dimensional Hierarchical Nanostructures. *Langmuir* **2010**, *26*, 12841−12848.

(11) Park, N. G.; van de Lagemaat, J.; Frank, A. J. Comparison of Dye-Sensitized Rutile- And Anatase-Based TiO_2 Solar Cells. *J. Phys. Chem. B* **2000**, *104*, 8989−8994.

(12) Testino, A.; Bellobono, I. R.; Buscaglia, V.; Canevali, C.; D'Arienzo, M.; Polizzi, S.; Scotti, R.; Morazzoni, F. Optimizing the Photocatalytic Properties of Hydrothermal TiO_2 by the Control of Phase Composition and Particle Morphology. A Systematic Approach. *J. Am. Chem. Soc.* **2007**, *129*, 3564−3575.

(13) Wold, A. Photocatalytic Properties of TiO_2. *Chem. Mater.* **1993**, *5*, 280−283.

(14) Wang, Y. W.; Zhang, L. Z.; Deng, K. J.; Chen, X. Y.; Zou, Z. G. Low Temperature Synthesis and Photocatalytic Activity of Rutile TiO_2 Nanorod Superstructures. *J. Phys. Chem. C* **2007**, *111*, 2709−2714.

(15) Yang, W. G.; Wan, F. R.; Wang, Y. L.; Jiang, C. H. Achievement of 6.03% Conversion Efficiency of Dye-Sensitized Solar Cells with Single-Crystalline Rutile TiO_2 Nanorod Photoanode. *Appl. Phys. Lett.* **2009**, *95*, 133121.

(16) Estruga, M.; Domingo, C.; Domenech, X.; Ayllon, J. A. Low Temperature N,N-Dimethylformamide-Assisted Synthesis and Characterization of Anatase-Rutile Biphasic Nanostructured Titania. *Nanotechnology* **2009**, *20*, 125604.

(17) Xin, X. K.; Wang, J.; Han, W.; Ye, M. D.; Lin, Z. Q. Dye-Sensitized Solar Cells Based on a Nanoparticle/Nanotube Bilayer Structure and Their Equivalent Circuit Analysis. *Nanoscale* **2012**, *4*, 964−969.

(18) Wu, J. M.; Zhang, T. W.; Zeng, Y. W.; Hayakawa, S.; Tsuru, K.; Osaka, A. Large-Scale Preparation of Ordered Titania Nanorods with Enhanced Photocatalytic Activity. *Langmuir* **2005**, *21*, 6995−7002.

(19) Shankar, K.; Basham, J. I.; Allam, N. K.; Varghese, O. K.; Mor, G. K.; Feng, X. J.; Paulose, M.; Seabold, J. A.; Choi, K. S.; Grimes, C. A. Recent Advances in the Use of TiO_2 Nanotube and Nanowire Arrays for Oxidative Photoelectrochemistry. *J. Phys. Chem. C* **2009**, *113*, 6327−6359.

(20) Isley, S. L.; Penn, R. L. Relative Brookite and Anatase Content in Sol−Gel-Synthesized Titanium Dioxide Nanoparticles. *J. Phys. Chem. B* **2006**, *110*, 15134−15139.

(21) Quinonez, C.; Vallejo, W.; Gordillo, G. Structural, Optical and Electrochemical Properties of TiO_2 Thin Films Grown by APCVD Method. *Appl. Surf. Sci.* **2010**, *256*, 4065−4071.

(22) Wang, J.; Lin, Z. Q. Freestanding TiO_2 Nanotube Arrays with Ultrahigh Aspect Ratio via Electrochemical Anodization. *Chem. Mater.* **2008**, *20*, 1257−1261.

(23) Wang, J.; Lin, Z. Q. Anodic Formation of Ordered TiO_2 Nanotube Arrays: Effects of Electrolyte Temperature and Anodization Potential. *J. Phys. Chem. C* **2009**, *113*, 4026−4030.

(24) Wang, J.; Lin, Z. Q. Dye-Sensitized TiO_2 Nanotube Solar Cells with Markedly Enhanced Performance via Rational Surface Engineering. *Chem. Mater.* **2010**, *22*, 579−584.

(25) Wang, J.; Zhao, L.; Lin, V. S. Y.; Lin, Z. Q. Formation of Various TiO_2 nanostructures from electrochemically anodized titanium. *J. Mater. Chem.* **2009**, *19*, 3682−3687.

(26) Wang, J.; Lin, Z. Q. Dye-Sensitized TiO_2 Nanotube Solar Cells: Rational Structural and Surface Engineering on TiO_2 Nanotubes. *Chem. Asian J.* **2012**, *7*, 2754−2762.

(27) Han, S. J.; Choi, S. H.; Kim, S. S.; Cho, M.; Jang, B.; Kim, D. Y.; Yoon, J.; Hyeon, T. Low-Temperature Synthesis of Highly Crystalline TiO_2 Nanocrystals and Their Application to Photocatalysis. *Small* **2005**, *1*, 812−816.

(28) Bakardjieva, S.; Stengl, V.; Szatmary, L.; Subrt, J.; Lukac, J.; Murafa, N.; Niznansky, D.; Cizek, K.; Jirkovsky, J.; Petrova, N. Transformation of Brookite-type TiO_2 Nanocrystals to Rutile: Correlation between Microstructure and Photoactivity. *J. Mater. Chem.* **2006**, *16*, 1709−1716.
(29) Chen, X.; Mao, S. S. Titanium Dioxide Nanomaterials: Synthesis, Properties, Modifications, And Applications. *Chem. Rev.* **2007**, *107*, 2891−2959.
(30) Lv, M.; Zheng, D.; Ye, M.; Sun, L.; Xiao, J.; Guo, W.; Lin, C. Densely Aligned Rutile TiO_2 Nanorod Arrays with High Surface Area for Efficient Dye-Sensitized Solar Cells. *Nanoscale* **2012**, *4*, 5872−5879.
(31) Lv, M. Q.; Zheng, D. J.; Ye, M. D.; Xiao, J.; Guo, W. X.; Lai, Y. K.; Sun, L.; Lin, C. J.; Zuo, J. Optimized Porous Rutile TiO_2 Nanorod Arrays for Enhancing the Efficiency of Dye-Sensitized Solar Cells. *Energy Environ. Sci.* **2013**, *6*, 1615−1622.
(32) Sang, Y.; Geng, B. Y.; Yang, J. Fabrication and Growth Mechanism of Three-Dimensional Spherical TiO_2 Architectures Consisting of TiO_2 Nanorods with {110} Exposed Facets. *Nanoscale* **2010**, *2*, 2109−2113.
(33) Zhou, J.; Zhao, G. L.; Song, B.; Han, G. R. Solvent-Controlled Synthesis of Three-Dimensional TiO_2 Nanostructures via a One-Step Solvothermal Route. *Crystengcomm* **2011**, *13*, 2294−2302.
(34) Yu, J.; Liu, W.; Yu, H. A One-Pot Approach to Hierarchically Nanoporous Titania Hollow Microspheres with High Photocatalytic Activity. *Cryst. Growth Des.* **2008**, *8*, 930−934.
(35) Liu, L.; Zhao, Y. P.; Liu, H. J.; Kou, H. Z.; Wang, Y. Q. Directed Growth of TiO_2 Nanorods into Microspheres. *Nanotechnology* **2006**, *17*, 5046−5050.
(36) Pan, J. H.; Zhang, X. W.; Du, A. J.; Sun, D. D.; Leckie, J. O. Self-Etching Reconstruction of Hierarchically Mesoporous F-TiO_2 Hollow Microspherical Photocatalyst for Concurrent Membrane Water Purifications. *J. Am. Chem. Soc.* **2008**, *130*, 11256.
(37) Zhao, Z.; Sun, Z.; Zhao, H.; Zheng, M.; Du, P.; Zhao, J.; Fan, H. Phase Control of Hierarchically Structured Mesoporous Anatase TiO_2 Microspheres Covered with {001} Facets. *J. Mater. Chem.* **2012**, *22*, 21965−21971.
(38) Mu, Q. H.; Li, Y. G.; Wang, H. Z.; Zhang, Q. H. Solvent-Controlled Formation and Photoelectrochemical Sensing Properties of 3-Dimensional TiO_2 Nanostructures. *Crystengcomm* **2011**, *13*, 6258−6264.
(39) Yu, J. G.; Fan, J. J.; Lv, K. L. Anatase TiO_2 Nanosheets with Exposed (001) Facets: Improved Photoelectric Conversion Efficiency in Dye-Sensitized Solar Cells. *Nanoscale* **2010**, *2*, 2144−2149.
(40) Liu, B.; Aydil, E. S. Growth of Oriented Single-Crystalline Rutile TiO_2 Nanorods on Transparent Conducting Substrates for Dye-Sensitized Solar Cells. *J. Am. Chem. Soc.* **2009**, *131*, 3985−3990.
(41) Cheng, H.; Ma, J.; Zhao, Z.; Qi, L. Hydrothermal Preparation of Uniform Nanosize Rutile and Anatase Particles. *Chem. Mater.* **1995**, *7*, 663−671.
(42) Lan, T.; Tang, X.; Fultz, B. Phonon Anharmonicity of Rutile TiO_2 Studied by Raman Spectrometry and Molecular Dynamics Simulations. *Phys. Rev. B* **2012**, *85*, 094305.
(43) Li, J.; Zeng, H. C. Hollowing Sn-Doped TiO_2 Nanospheres via Ostwald Ripening. *J. Am. Chem. Soc.* **2007**, *129*, 15839−15847.
(44) Cui, Y. M.; Liu, L.; Li, B.; Zhou, X. F.; Xu, N. P. Fabrication of Tunable Core−Shell Structured TiO_2 Mesoporous Microspheres Using Linear Polymer Polyethylene Glycol as Templates. *J. Phys. Chem. C* **2010**, *114*, 2434−2439.
(45) Dong, W.; Li, B.; Li, Y.; Wang, X.; An, L.; Li, C.; Chen, B.; Wang, G.; Shi, Z. General Approach to Well-Defined Perovskite $MTiO_3$ (M = Ba, Sr, Ca, and Mg) Nanostructures. *J. Phys. Chem. C* **2011**, *115*, 3918−3925.
(46) Li, Y.; Gao, X. P.; Li, G. R.; Pan, G. L.; Yan, T. Y.; Zhu, H. Y. Titanate Nanofiber Reactivity: Fabrication of $MTiO_3$ (M = Ca, Sr, and Ba) Perovskite Oxides. *J. Phys. Chem. C* **2009**, *113*, 4386−4394.
(47) Morgan, B. J.; Watson, G. W. A Density Functional Theory plus U Study of Oxygen Vacancy Formation at the (110), (100), (101), and (001) Surfaces of Rutile TiO_2. *J. Phys. Chem. C* **2009**, *113*, 7322−7328.
(48) Ye, M. D.; Liu, H. Y.; Lin, C. J.; Lin, Z. Q. Hierarchical Rutile TiO_2 Flower Cluster-Based High Efficiency Dye-Sensitized Solar Cells via Direct Hydrothermal Growth on Conducting Substrates. *Small* **2013**, *9*, 312−321.
(49) Xu, X.; Zhao, Y.; Lai, Q.; Hao, Y. Effect of Polyethylene Glycol on Phase and Morphology of Calcium Carbonate. *J. Appl. Polym. Sci.* **2011**, *119*, 319−324.
(50) Zhou, X. F.; Chen, S. Y.; Zhang, D. Y.; Guo, X. F.; Ding, W. P.; Chen, Y. Microsphere Organization of Nanorods Directed by PEG Linear Polymer. *Langmuir* **2006**, *22*, 1383−1387.
(51) Xu, X. Y.; Zhao, Y.; Lai, Q. Y.; Hao, Y. J. Effect of Polyethylene Glycol on Phase and Morphology of Calcium Carbonate. *J. Appl. Polym. Sci.* **2011**, *119*, 319−324.
(52) Zeng, Y.; Zhang, T.; Wang, L. J.; Wang, R. Synthesis and Ethanol Sensing Properties of Self-Assembled Monocrystalline ZnO Nanorod Bundles by Poly(ethylene glycol)-Assisted Hydrothermal Process. *J. Phys. Chem. C* **2009**, *113*, 3442−3448.
(53) Sun, A. H.; Guo, P. J.; Li, Z. X.; Li, Y.; Cui, P. Low Temperature Synthesis of Anatase and Rutile Titania Nanopowders by Hydrolysis of $TiCl_4$ Using Ammonia Gas. *J. Alloy. Compd.* **2009**, *481*, 605−609.
(54) Liu, C. X.; Zhang, L.; Deng, J. G.; Mu, Q.; Dai, H. X.; He, H. Surfactant-Aided Hydrothermal Synthesis and Carbon Dioxide Adsorption Behavior of Three-Dimensionally Mesoporous Calcium Oxide Single-Crystallites with Tri-, Tetra-, and Hexagonal Morphologies. *J. Phys. Chem. C* **2008**, *112*, 19248−19256.
(55) Yu, J. G.; Qi, L. F. Template-Free Fabrication of Hierarchically Flower-Like Tungsten Trioxide Assemblies with Enhanced Visible-Light-Driven Photocatalytic Activity. *J. Hazard. Mater.* **2009**, *169*, 221−227.
(56) Zhu, K.; Neale, N. R.; Halverson, A. F.; Kim, J. Y.; Frank, A. J. Effects of Annealing Temperature on the Charge-Collection and Light-Harvesting Properties of TiO_2 Nanotube-Based Dye-Sensitized Solar Cells. *J. Phys. Chem. C* **2010**, *114*, 13433−13441.